Determination of critical length scales and the limit of metastability in phase separating polymer blends

A. A. Lefebvre and J. H. Lee
Department of Chemical Engineering, University of California, Berkeley, California 94720

N. P. Balsara
Department of Chemical Engineering, University of California, Berkeley, California 94720 and Materials Sciences Division, Lawrence Berkeley National Laboratory, University of California, Berkeley, California 94720

C. Vaidyanathan
Department of Chemical Engineering, Chemistry, and Materials Science, Polytechnic University, Brooklyn, New York 11201

(Received 20 June 2002; accepted 9 August 2002)

Liquid–liquid phase separation in polymethylbutylene/polyethylbutylene blends near the metastability limit was studied using small angle neutron scattering (SANS). Our objective was to study the relationship between quench depth and R_c, the lower limit for the length scale of the structures formed during the early stages of the phase transition (nuclei). During the early stage of phase separation, the SANS profiles merged at a time-independent critical scattering vector, q_c. We discuss different methods for estimating q_c, and present arguments for the scaling relationship, $R_c \sim 1/q_c$. The theory of Cahn and Hilliard predicts that in metastable blends R_c increases with increasing quench depth, and diverges at the spinodal. In contrast, our experimental measurements showed R_c increases with decreasing quench depth, and the location of the point where R_c diverges lies between the binodal and the spinodal. Some aspects of our results are addressed in recent theoretical work of Wang and Wood [J. Chem. Phys. **117**, 481 (2002)], wherein the effects of fluctuations on the binodal and spinodal curves in polymer blends are incorporated. © *2002 American Institute of Physics.* [DOI: 10.1063/1.1511512]

I. INTRODUCTION

Nucleation and growth is the universal process that underlies phase transformations from a metastable nonequilibrium state to a stable equilibrium state.[1–20] Classical nucleation theory,[1,2] which has been used to describe diverse phenomena such as crystallization, boiling, and liquid–liquid phase separation, is based on the assumption that these phase transitions are triggered by the formation of microscopic nuclei. For simplicity, we restrict our attention to homogeneous nucleation, assuming that foreign objects that are in contact with the system (dust, container walls, etc.) do not effect nucleation. Growth of the new phase requires spontaneous formation of nuclei that are larger than a critical size. We refer to this critical length scale as R_c. Classical theory assumes that the nuclei are small regions in space that have all of the characteristics of the stable state. The relevant characteristics, which include concentration, density, crystal structure, etc., depend on the particular phase transition under consideration. We refer to these collective characteristics as ''composition'' of the nuclei. Nuclei with sizes smaller than R_c or with compositions that are different from that of the new equilibrium phase are nonviable and are predicted to decay. The evolution of a metastable state into a stable one is thus characterized by a complex collection of structures with differing sizes and compositions.

If the decay of nonviable nuclei is rapid so that their concentration is negligible, then proving the existence of a critical length scale requires demonstrating the *absence* of growing structures with sizes smaller than R_c, regardless of their composition. This is a nontrivial task because traditional experimental methods (e.g., microscopy and scattering) are mainly used to prove the *presence* of certain structures.

Recent experiments have shown that the size of the critical nucleus can be measured in position space by time-resolved microscopy. Yau *et al.* studied crystallization of proteins from supersaturated solutions.[19] In these experiments, the characteristics of crystallites that happened to lie on the bottom surface of the cell were observed by atomic force microscopy. It was found that crystallites with a certain composition, size, and shape grew while others decayed. Gasser *et al.* examined the formation of crystalline nuclei in a concentrated hard sphere suspension.[20] The state of a hard sphere suspension is independent of temperature or pressure. Gasser *et al.* thus prepared a metastable ''homogeneous'' state by shearing the sample. The growth of the crystallites was then observed by laser scanning confocal microscopy after turning off the shear flow. They found that the larger crystallites grew while the smaller ones decayed. While these novel experiments[19,20] provide vivid evidence for the existence of a critical length scale, some questions remain. The interpretation of results obtained by Yau *et al.* rests on the assumption that the nucleation events occurring in the bulk and those occurring on the cell surface are identical. The

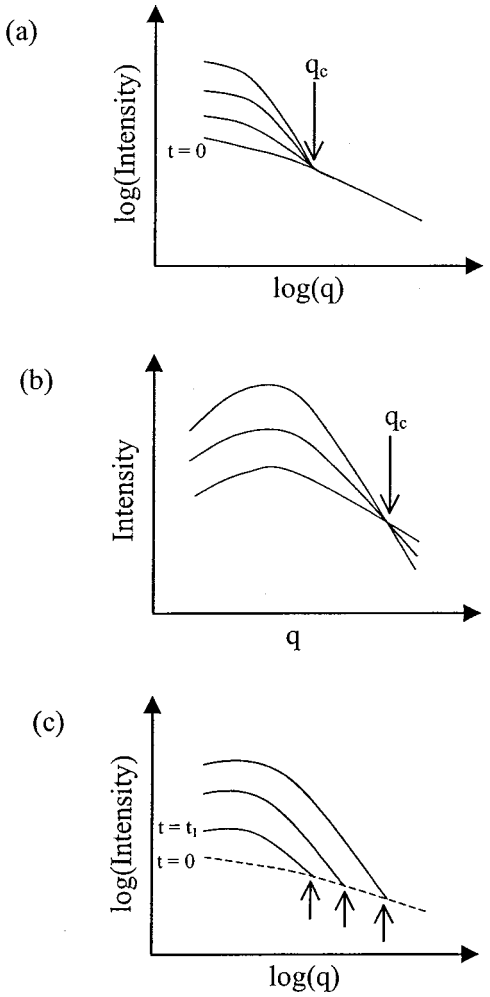

FIG. 1. Schematic time-dependent scattering profiles (intensity vs scattering vector) for blends where q_c is given by the (a) merging or (b) intersection of scattering curves. (c) Case where the merge point is time-dependent for times greater than t_1.

presence of a sizable concentration of nonviable (smaller than R_c) nuclei in the colloidal samples suggests that the shear melting did not eliminate all of the ordered crystallites. The role of the remaining crystallites on nucleation is unclear at this point.

In previous studies, our group has demonstrated that R_c during liquid–liquid phase separation in blends of high molecular weight polymers can be measured in reciprocal space by time-resolved small angle neutron scattering (SANS).[16,17] The composition of the nuclei of binary incompressible liquids is specified by one parameter, namely, the concentration of one of the components. We found that SANS profiles during the early stages of phase separation merged at a characteristic scattering vector q_c, as shown schematically in Fig. 1(a). The formation and growth of structures with size R will lead to a scattering increase at $q \approx 1/R$. The composition of the structures (relative to the homogeneous background) will only effect the magnitude of the scattering increase. The time independence of the scattering intensity at $q > q_c$ thus indicates the absence of growing structures with length scales smaller than $1/q_c$, regardless of their composition. The size of the critical nucleus, ignoring a constant prefactor, is thus $1/q_c$.[21]

The applicability of nucleation theory ends at the spinodal, the point at which the initial state of the system is unstable to infinitesimal perturbations. The kinetics of liquid–liquid phase separation in unstable mixtures is described by Cahn's theory of spinodal decomposition.[22,23] The time dependence of the scattering profiles obtained during spinodal decomposition depends on quench depth as well as the mutual diffusion coefficient, D. During the early stages of phase separation concentration fluctuations of a certain characteristic wavelength grow most rapidly. The standard signature of spinodal decomposition is a scattering peak at a scattering vector that we call q_p. This scattering peak has received considerable attention, and has been identified in a wide variety of systems such as metals, glasses, polymer blends, etc.[3,24–34]

There is, however, another feature of spinodal decomposition predicted by Cahn that has received much less attention. It is the fact that concentration fluctuations with characteristic wavelengths smaller than a particular cutoff are predicted to decay with time.[22] This yields a critical scattering vector, q_c. Thermodynamically unstable systems are characterized by a singularity in the structure factor $S(q)$ located at $q = q_c$. Thus, q_c depends only on thermodynamics. In contrast, q_p depends on both thermodynamics (quench depth) and kinetics (diffusion coefficient). It is thus more straightforward to compare q_c with theoretical predictions.

In simple mixtures, where $1/q_c$ is much larger than molecular length scales and the diffusion coefficient can be regarded as a constant, $q_c = \sqrt{2} q_p$. In systems such as polymers, where q_c can be comparable to molecular length scales,[35–37] the diffusion coefficient cannot be treated as a constant. This leads to more complicated relationships between q_c and q_p.

The scattering signature of q_c is not entirely clear at this point. In some papers, e.g., Ref. 22, it has been proposed that the time-dependent scattering curves should cross at q_c, as shown schematically in Fig. 1(b). In other words, the scattering intensity would increase with time at $q < q_c$ and decrease with time at $q > q_c$. However, the data shown in Ref. 22 to support this notion was obtained in a metallic blend during the late stages of spinodal decomposition. Since the scattering intensity of the prequenched state will generally be lower than that of the quenched state, there appears to be no mechanism for a decrease in scattering at $q > q_c$ within Cahn's theory. In this case one would expect the scattering curves to merge at q_c, as shown in Fig. 1(a), rather than intersect at q_c, as shown in Fig. 1(b). We may thus observe a merging of scattering curves [Fig. 1(a)] regardless of whether the mixture is phase separating by nucleation and growth or spinodal decomposition.

While we have provided plausible arguments for interpreting the merging of scattering curves in terms of a critical length scale, we have not provided rigorous proof that this is the case. One might argue, for instance, that the scattering profiles that characterize the emerging phase separated structures (e.g., critical nuclei) are much larger (on an equal volume basis) than that from the concentration fluctuations in

TABLE I. Characteristics of polymers.

Polymer	Density (g/cm^3)	Average number of deuterium atoms per 6 carbon atoms	Weight averaged molecular weight (g/mol)	Polydispersity index	R_g (nm)
PMB1	0.9300	7.33	1.8×10^5	1.07	16.7
PMB2	0.9192	6.26	1.7×10^5	1.02	16.2
PEB1	0.8628	0	2.2×10^5	1.08	16.6
PEB2	0.8637	0	2.2×10^5	1.08	16.6

the prequenched mixture, and that this scattering signal is not detected initially because the amount of phase separated material is extremely small. In this scenario, the measured scattering profiles would become time-dependent when scattering from the phase separated structures begins to overwhelm the scattering from the homogeneous prequenched state. This is depicted in Fig. 1(c), where the background scattering from the prequenched state is shown by the dashed curve and t_1 is the time when the scattering from domains is first detected. The total scattering is then approximately given by the sum of the scattering from the domains [solid curve in Fig. 1(c)] and the background (dashed curve). If this were the case, then the merge point would shift to larger q with increasing time, as shown by the arrows in Fig. 1(c). This is because scattering from the domains occupies an increasing portion of the q-window with increasing time, due to increases in domain size and concentration. It is clear that the critical nucleus size can be obtained from q_c only if q_c is time-independent, as shown in Fig. 1(a).

In this paper, we discuss the determination of q_c from time-resolved SANS data obtained from binary polymer blends quenched into the two-phase region of the phase diagram. We focus on off-critical blends near the limit of metastability due to our interest in studying the initial stages of nucleation. One of our objectives is to distinguish between the 3 scenarios shown in Fig. 1. We describe connections between our results and recent theoretical work on the thermodynamics of binary polymer blends by Wang and Wood.[12,39] In the paper that follows,[38] we analyze the time dependence of the scattering intensity at $q<q_c$. These papers are part of a series on the subject of phase separation kinetics in polymer blends.[16–18,32,33] Our early results[17,18,32,33] could not be compared directly with theory because the experiments were conducted on multicomponent mixtures and theories on phase separation kinetics are largely restricted to binary mixtures.

II. EXPERIMENT

Nearly monodisperse model polyolefins were synthesized following the methods given in Refs. 40–42. Partially deuterated polymethylbutylenes (PMB1 and PMB2) and fully hydrogeneous polyethylbutylenes (PEB1 and PEB2) were synthesized and characterized using methods described in Refs. 43 and 47. The characteristics of the polymers are given in Table I. Binary blends of PMB/PEB were made by dissolving the components in cyclohexane and then drying the blends to a constant weight in a vacuum oven at 80 °C. The volume fractions of PMB in the blends used in these experiments are given in Table II. Preliminary results of kinetic experiments on blends B1 and B2 are given in Ref. 16. Kinetic experiments performed on blend B3 have not been previously published.

TABLE II. Blend components and compositions.

Sample	Components A	Components B	ϕ_{PMB}
B1	PMB1	PEB1	0.161
B2	PMB1	PEB1	0.099
B3	PMB2	PEB2	0.160

Small angle neutron scattering experiments (SANS) were performed on the NG3 beamline at the National Institute of Standards and Technology in Gaithersburg, MD, during four 4-day experimental runs. The data acquisition protocols were slightly different from run to run, due to changes (improvements) in the SANS instrument and a better understanding of phase separation kinetics.

The samples were housed in two different versions of the NIST pressure cell. The pressure cell utilized for the experiments on B1 and B2 is described in Ref. 44 and had a pressure range of 0.01–1.00 kbar. The pressure cell utilized for the experiments on B3 had a range of 0.03–3.10 kbar, as described in Ref. 45. The time required to change the sample pressure (i.e., reach within 1% of the target pressure) ranged from 1 to 14 min for B1 and B2, and from 1 to 4 min for B3.

The SANS data were obtained using two instrument configurations, one with an incident neutron beam with wavelength $\lambda=6$ Å and the other with $\lambda=14$ Å (see Ref. 47 for details). The scattering data were collected using a 128×128 pixel two-dimensional detector. The data obtained in the $\lambda=6$ Å configuration were corrected for background scattering, empty cell scattering, and detector sensitivity and converted to absolute scattering intensity, $I(q)$, using methods and secondary standards described in Ref. 46. The time-resolved data were obtained using the $\lambda=14$ Å configuration. The data from the B1 and B2 blends in this configuration were not corrected or converted to absolute intensity. The time-dependent SANS profiles ($\lambda=14$ Å) of B3 were corrected for background scattering, empty cell scattering, incoherent scattering and detector sensitivity and converted to absolute scattering intensity. The scaling factor for converting the corrected scattering intensity in the $\lambda=14$ Å configuration to absolute scattering intensity was obtained by matching the SANS profile of the secondary standard in this configuration to that obtained in the $\lambda=6$ Å configuration, in the range of q values accessible to both configurations.[47] The scaling was confirmed by comparing the SANS profile measured from B3 in the single-phase region in both configurations. All of the scattering profiles were azimuthally symmetric. We thus report the azimuthally averaged scattering intensity as a function of q [$q=4\pi\sin(\theta/2)/\lambda$, θ is the scattering angle].

TABLE III. The dependence of χ on temperature at selected pressures for the B1 and B2 blends with a reference volume of 100 Å^3. $\chi = A + B/T + C/T^2$.

Pressure (kbar)	B1			B2			B3		
	A	B(K)	C(K^2)	A	B(K)	C(K^2)	A	B(K)	C(K^2)
0.19	0.00181	−1.402	355.33						
0.27	0.00196	−1.543	387.96						
0.34	0.00210	−1.666	416.52						
0.38	0.00218	−1.736	432.84						
0.43	0.00227	−1.824	453.24						
0.51	0.00243	−1.964	485.88						
0.86	0.00271	−2.276	570.96				0.00168	−1.405	378.30
1.00				0.00221	−1.969	521.46			
1.24							0.00117	−1.108	343.12
1.66							0.000674	−0.835	315.54
2.00							0.000275	−0.613	293.21
3.10							−0.00241	1.226	0

III. EXPERIMENTAL RESULTS

The equilibrium thermodynamic properties of the PMB/PEB blends used in this study have been thoroughly investigated.[44,45,48–50] The pressure dependence of the mean-field binodal (T_b) and spinodal (T_s) temperatures of the blends were calculated using Flory–Huggins theory.[44,45] Most of our quenches were located between T_b and T_s. All of the quenches on the B2 blend were performed at 1.00 kbar. Quenches on B2 are thus referred to by the quench temperature only. All of the quenches on the B1 and B3 blends were performed at the same temperature: 48 °C for B1 and 58 °C for B3. Quenches on B1 and B3 are thus referred to by the quench pressure only.

The samples were prepared for each phase separation experiment using a two-step procedure: a homogenization step followed by a cooling step. The homogenization step consisted of heating the sample well above the binodal at the lowest accessible pressure (109 °C and 0.01 kbar for B1, 79 °C and 0.01 kbar for B2, and 106 °C and 0.03 kbar for B3) for a minimum of 15 min, to erase the effect of thermal and pressure history. For each blend, homogenization was then verified by ensuring that the measured SANS profiles at the end of each homogenization step were the same. For B3, we compared the measured $I(q)$ with theoretical predictions, based on the random phase approximation (RPA),[35]

$$I(q) = \left(\frac{b_1}{v_1} - \frac{b_2}{v_2}\right)^2 \left(\frac{1}{N_1 v_1 \phi_1 P_1(q)} + \frac{1}{N_2 v_2 \phi_2 P_2(q)} - \frac{2\chi}{v_0}\right)^{-1}, \quad (1)$$

where b_i is the neutron scattering length of the monomer in polymer chain i with a monomer volume v_i, N_i is the number of monomer units with a volume v_i in polymer chain i, ϕ_i is the volume fraction of polymer i, P_i is the Debye function of polymer chain i, χ is the Flory–Huggins interaction parameter, and v_0 is a reference volume, which for this work is equal to 100 Å^3. The Debye function is given by

$$P_i(q) = \frac{2}{x^2}(e^{-x} + x - 1), \quad (2)$$

where $x = q^2 R_{gi}^2$, $R_{gi}^2 = N_i l_{i,\mathrm{ref}}^2/6$ and $l_{i,\mathrm{ref}}$ is the statistical segment length of polymer i.

Previous work on PMB/PEB blends indicated that the dependence of χ on component molecular weight and blend composition was within experimental error.[44,45,48–51] However, χ determined from off-critical blends is subject to substantial errors (±20%) due mainly to uncertainties in molecular weight and instrument calibration. To minimize the effect of these errors, the same blend used for the phase separation experiments was also used to determine χ as a function of T and P. At fixed pressure, we find that χ is a quadratic function of $1/T$ ($\chi = A + B/T + C/T^2$). At very high pressures (3.10 kbar) C approaches zero.[44,45,48–51] The values of A, B, and C at the relevant pressures for each of the blends are given in Table III. The other parameters required to compute $I(q)$ using Eq. (1) were obtained by methods described in Ref. 43 and are given in Table IV.

In Fig. 2(a) we show SANS data obtained after each homogenization of B3 at 106 °C and 0.03 kbar. It is evident from Fig. 2(a) that all of the profiles obtained after homogenization are within experimental error. Also shown in Fig. 2(a) is the theoretical $I(q)$ of the blend calculated at 106 °C and 0.03 kbar (solid curve), which is in good agreement with the data. After homogenization, the sample was then cooled at 0.03 kbar to 58 °C. The data obtained after the cooling step are shown in Fig. 2(b). Again we find reasonable agreement between the data sets and the RPA calculation at 0.03 kbar to 58 °C (solid curve), indicating that no phase separation takes place after the cooling step. It is important to note that the agreement between theory and experiment seen in Figs. 2(a) and 2(b) is obtained without any adjustable parameters. The increased scatter in the data in Fig. 2(b) is due to a change in SANS instrument configuration for the phase separation experiments that commence right after the cooling step.

Phase separation was initiated at time zero ($t = 0$) by a command to the pressure controller. The time dependence of the SANS profiles obtained during phase separation from

TABLE IV. Parameters used for RPA and pseudospinodal calculations.

Parameter	PMB1	PMB2	PEB1	PEB2
N_i	2465	2312	2630	2630
v_i (Å^3/monomer)	136.2	136.1	162.0	162.0
$l_{i,\mathrm{ref}}$ (Å)	8.26	8.26	7.93	7.93
b_i (Å)	5.95×10^{-4}	4.90×10^{-4}	-4.98×10^{-5}	-4.98×10^{-5}
l_i, (Å)	2.00	2.00	2.58	2.58

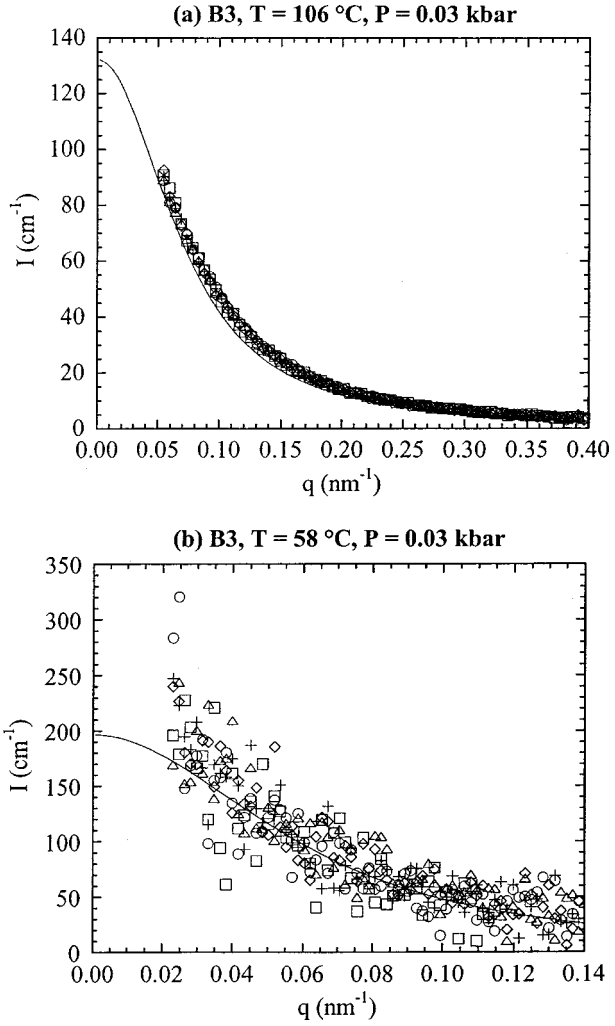

FIG. 2. The scattering intensity, I, vs q for the B3 blend after homogenization at (a) 106 °C and 0.03 kbar, and (b) 58 °C and 0.03 kbar just before initiating the pressure quench. Circles: 0.86 kbar, diamonds: 1.24 kbar, pluses: 1.66 kbar, triangles: 2.00 kbar, and squares: 3.10 kbar quench. The solid curves were calculated using Eq. (1).

selected quenches are shown in Fig. 3. In Fig. 3(a) we show typical data obtained during deep quenches (B1, $P=0.86$ kbar). Here the scattering intensity increases rapidly and a peak is seen to develop at $q=0.035\ \mathrm{nm}^{-1}$. In contrast, experiments at intermediate quench depths led to scattering profiles that are monotonic functions of q. An example of this is shown in Fig. 3(b) where we show data obtained from B1 during the 0.19 kbar quench. Data obtained from a very shallow quench is shown in Fig. 3(c) where we show data from B2 at 45 °C. Here we see only a slight increase in the low q scattering ($q<0.030\ \mathrm{nm}^{-1}$). Decreasing the quench depth further results in no phase separation. This is shown in Fig. 3(d) where we show data obtained from B2 at 65 °C, where the scattering curves at $t=3$ and 975 min are within experimental error.

The time dependence of the intensity, I, at $q=0.021\ \mathrm{nm}^{-1}$, the lowest accessible q, for the 40 °C quench on the B2 sample is shown in Fig. 4(a). We see three distinct stages: a stage where I increases rapidly ($t<92$ min), followed by a stage where I increases slowly ($92\leqslant t\leqslant 444$ min), and finally a stage wherein I increases rapidly again ($t>444$ min). In Ref. 17, we argued that the rapid increase seen in I in the very early stages of phase separation in shallow quenches is due to the fact that a finite amount of time is required for the fluctuations to adjust to a change in pressure. We thus called this the fluctuation relaxation stage. The end of the fluctuation relaxation stage was determined by a *least-squares two lines procedure*. The procedure is as follows: the data at $t\leqslant 444$ min were divided into two groups (short time and long time) and the best least-squares lines were drawn through the two data sets. The point of division between the short time and long time regimes was varied systematically. The pair of lines, which minimized the sum of the square of the residuals, was chosen to describe the data. The end of the fluctuation relaxation stage is the time of the first data point in the long time group and is indicated by τ_F in Fig. 4(a). We observed this fluctuation relaxation process only in the shallowest quenches (i.e., quenches on the B2 sample to 45 °C, 40 °C, 35 °C,[52] and the 1.24 kbar quench on the B3 blend), where phase separation happens relatively slowly. In the deeper quenches, it is likely that this process is overwhelmed by rapid phase separation. An example of such data is shown in Fig. 4(b) where we show data obtained from one of the quenches on B2 at 35 °C. Here we see an early stage where I increases slowly with time ($t<280$ min) followed by a late stage where I increases rapidly with time ($t>280$ min). Since we are interested in studying the early stages of phase separation, we do not discuss the data at $t<\tau_F$ in the remainder of this paper.

The crossover from the early stage where I increases slowly with time to the late stage where I increases rapidly with time is more gradual than the crossover from the fluctuation relaxation stage to the early stage (see Fig. 4). The time signifying the end of the early stage is given the symbol τ_E. We estimated τ_E as follows: We first compute the mean intensity, $\overline{I(t)}$, and the standard deviation about $\overline{I(t)}$ at $q=0.021\ \mathrm{nm}^{-1}$, σ_E, defined as

$$\sigma_E=\sqrt{\frac{\Sigma_{\tau_F}^{\tau_E}[I(t)-\overline{I(t)}]^2}{n-1}} \tag{3}$$

for at least 5 data points ($n\geqslant 5$). The sum of the average plus 2 standard deviations about the mean, $S_2=\overline{I(t)}+2\sigma_E$ is calculated. The next data point is then added to the set and $\overline{I(t)}$, σ_E, and thus S_2 are recalculated. If the value of $I(t)$ for the new data point is smaller than S_2, another point is added to the set and the procedure repeated. If the value of $I(t)$ for the new data point and for all times larger than t is larger than S_2, then the previous point is designated τ_E, the end of the nucleation stage. The value of τ_E thus obtained for B2 at 40 °C and 35 °C are shown in Figs. 4(a) and 4(b). The dashed lines in these figures represent 2 standard deviations above and below $\overline{I(t)}$ during the early stage of phase separation. We refer to this procedure for identifying the cross-over as the *standard deviation procedure*.

In Fig. 5 we show the quench depth dependence of τ_E for the blends from the quenches into the metastable region of the phase diagram only. We have used χ/χ_s to indicate the quench depth, where χ is the Flory–Huggins interaction pa-

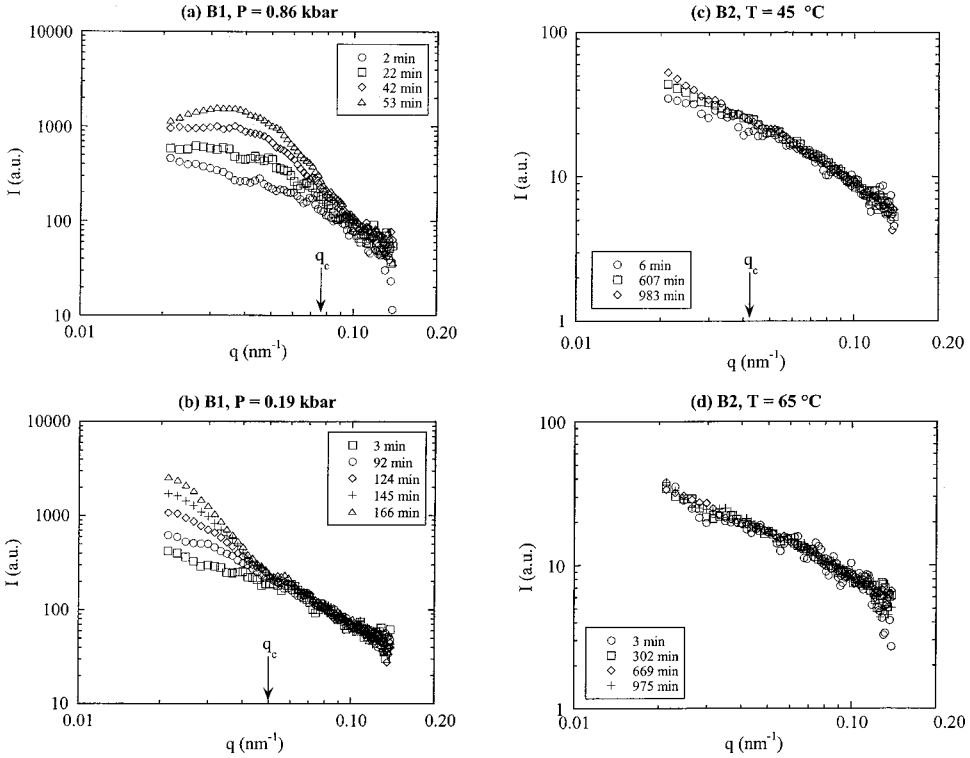

FIG. 3. The time dependent scattering intensity, I, vs q obtained from the B1 sample at 48 °C and (a) 0.86 kbar, and (b) 0.19 kbar and the B2 blend at 1.00 kbar and (c) 45 °C, and (d) 65 °C. The arrows indicate the location of q_c during the early stage of phase separation.

rameter at the T and P values at which the phase separation experiments were carried out, and χ_s is the value of χ at the spinodal computed at the quench pressure.[16] The correspondence between the quench T and P, and χ/χ_s for each of the blends is given in Table V. It is evident in Fig. 5 that to a reasonable approximation, τ_E decreases exponentially with increasing quench depth. The curve through the data is the least-squares fit of an empirical equation,

$$\frac{\tau_E}{\tau_0} = \exp\left[-E\left(\frac{\chi}{\chi_s}-1\right)\right]-1. \tag{4}$$

Since nucleation is an activated process, the time to cross the activation barrier, τ_E, should depend exponentially on quench depth. At the spinodal ($\chi=\chi_s$), the barrier for nucleation should vanish and τ_E should approach a microscopic time scale that is much smaller than experimentally accessible time scales. Thus τ_E is set to zero at $\chi=\chi_s$ in Eq. (4). In Eq. (4), E is a parameter that relates the quench depth to the nucleation barrier. The fit in Fig. 5 gives $\tau_0=28.8$ min and $E=10.7$.

We now focus exclusively on the scattering data obtained during the early stage of phase separation defined as $t\leqslant\tau_E$, or $\tau_F\leqslant t\leqslant\tau_E$ if $\tau_F>0$. A visual examination of the data in Figs. 3(a)–3(c) suggests that there exists a critical scattering vector q_c such that I increases with time at $q<q_c$ and I is independent of time at $q>q_c$. These critical scattering vectors are shown by arrows in Fig. 3. We now describe the procedure that was used to arrive at q_c.

A least-squares line was used to describe the time dependence of I at all q during the early stage. In Fig. 6(a) we show an example of such data, obtained from B3 at $P=1.66$ kbar. The slope of these lines gives dI/dt. The q-dependence of dI/dt, is shown in Fig. 6(b). We find that dI/dt is large at low q, decreases rapidly with increasing q, and fluctuates near zero at high q. In the absence of noise, we would expect dI/dt to be identically zero at $q>q_c$.

To obtain the first estimate of q_c, which we call q_{c1}, we use the same standard deviation procedure as was used to estimate τ_E. We calculate S_2 for $0.11\,\mathrm{nm}^{-1}\geqslant q\geqslant 0.10\,\mathrm{nm}^{-1}$ and then add subsequent data points as we move from high to low q.[53] The location of q_{c1} is designated as the q, where dI/dt at all $q\leqslant q_{c1}$ is greater than S_2 for $q>q_{c1}$. In Fig. 6(b), the dashed lines above and below the high q data represent 2 standard deviations above and below the mean dI/dt for $q>q_{c1}$. The second estimate of q_c, which we call q_{c2}, is obtained by the least-squares two lines procedure (the same method that was used to determine τ_F). The solid lines in Fig. 6(b) show the results of this procedure.[54] The location of the intersection of the two lines gives q_{c2}. The third method was also based on the least-squares two lines procedure except the slope of the second line, used to fit the high q data, was set to zero. The solid lines in the inset in Fig. 6(b) show the results of this procedure. The arrows in Fig. 6(b) and the inset indicate the location of q_{c1}, q_{c2}, and q_{c3}.

We also used the standard deviation procedure to obtain three additional estimates of q_c. We calculated $\sigma(q)$, the standard deviation of I at each q during the early stage,

$$\sigma(q)=\sqrt{\frac{\sum_{\tau_F}^{\tau_E}[I(t)-\overline{I(t)}]^2}{m-1}}, \tag{5}$$

where $I(q,t)$ is the intensity at each time during the early stage for a given q, $\overline{I(q,t)}$ is the mean intensity at that q during the early stage, and m is the number of scattering profiles measured during the early stage. The q dependence

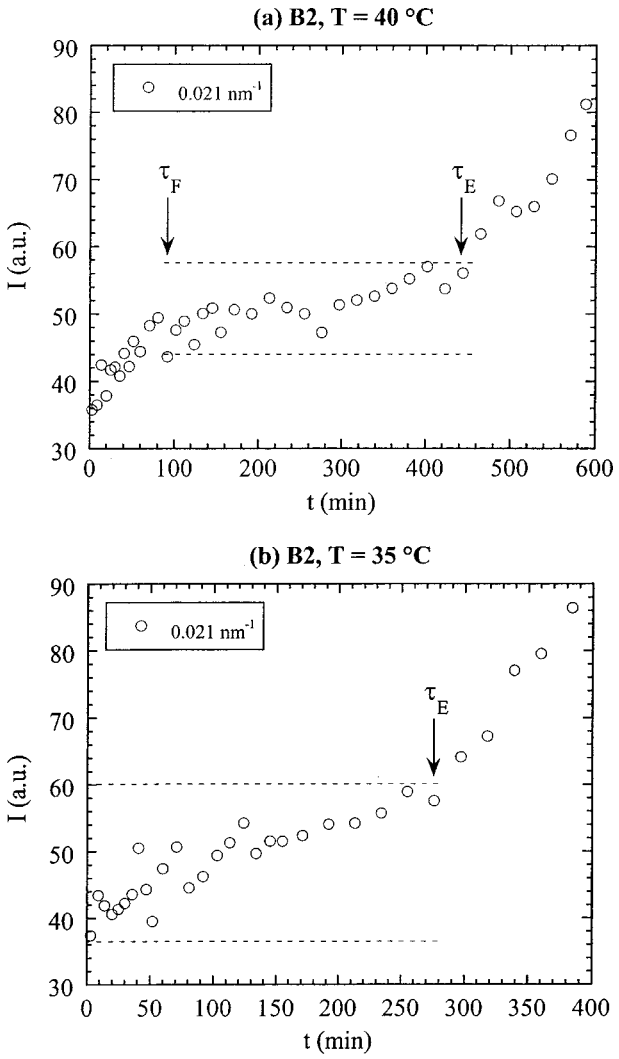

FIG. 4. The scattering intensity, I, vs time at $q=0.021\ \mathrm{nm}^{-1}$ for (a) the 40 °C and (b) a 35 °C quench on the B2 sample. The dashed lines are equal to twice the standard deviation about the mean intensity during the early stage. The arrows indicate τ_F, the end of the fluctuation relaxation stage [(a) only], and τ_E, the end of the early stage.

of σ for the 1.66 kbar quench on B3 is shown in Fig. 7. We used the standard deviation procedure on $\sigma(q)$ to obtain q_{c4}, the least-squares two lines procedure to estimate q_{c5} and the least-squares two lines procedure with zero slope to obtain q_{c6}. The results of these procedures on the B2 data at 1.66 kbar are shown by the arrows in Fig. 7.

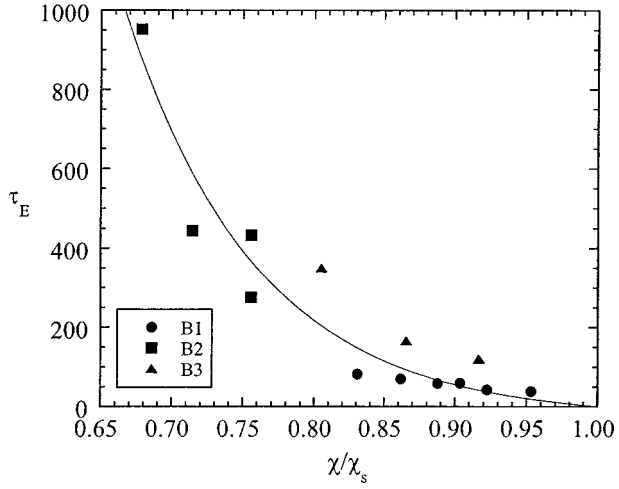

FIG. 5. The quench depth dependence of τ_E for B1, B2, and B3. The solid curve through the data is the best least-squares fit of $\tau_E/\tau_0=\exp[-B(\chi/\chi_s-1)]$-1, where $\tau_0=28.8$ min and $B=10.7$.

We obtained six estimates of q_c by repeating the above described procedures on all of the data sets. In most cases, the least-squares two lines procedure with varying slopes gave the smallest q_c (q_{c2} and q_{c5}), while the standard deviation procedures gave the largest value of q_c (q_{c1} and q_{c4}). The locations of q_c as determined from these six methods are then averaged to yield our best estimate of q_c; it is this averaged q_c that is shown by the arrows in Fig. 3.

Until this point we have focused on the data obtained during the early stages of phase separation. We stopped most of our experiments when rapid phase separation began (i.e., near $t=\tau_E$). However, in a few cases, e.g., B1 at 0.34 kbar, phase separation was allowed to proceed well past the early stage. Figure 8(a) shows scattering profiles at selected times obtained during this experiment. τ_E for this quench is 58 min and q_c obtained by the methods given above is indicated in Fig. 8(a). It is evident from a visual inspection of Fig. 8(a) that the merge points, as indicated by the arrows, at $t>\tau_E$ become time dependent. To quantify the change in the merge point with time, we calculated ΔI, the difference between the scattering intensity at a given time, $I(t)$, and the scattering intensity at the first time data was recorded, $I(t=2\ \mathrm{min})$. We used the standard deviation method on the q-dependence of ΔI to obtain the q value at which the $I(t)$ data merged with the $I(t=2\ \mathrm{min})$ data. We use the symbol

TABLE V. Value of χ/χ_s for each quench.

B1			B2			B3		
Quench T (°C)	Quench P (kbar)	χ/χ_s	Quench T (°C)	Quench P (kbar)	χ/χ_s	Quench T (°C)	Quench P (kbar)	χ/χ_s
48	0.19	0.83	65	1.00	0.55	58	0.86	0.75
48	0.27	0.86	45	1.00	0.68	58	1.24	0.81
48	0.34	0.89	40	1.00	0.71	58	1.66	0.87
48	0.38	0.90	35	1.00	0.76	58	2.00	0.92
48	0.43	0.92				58	3.10	1.05
48	0.51	0.95						
48	0.86	1.06						

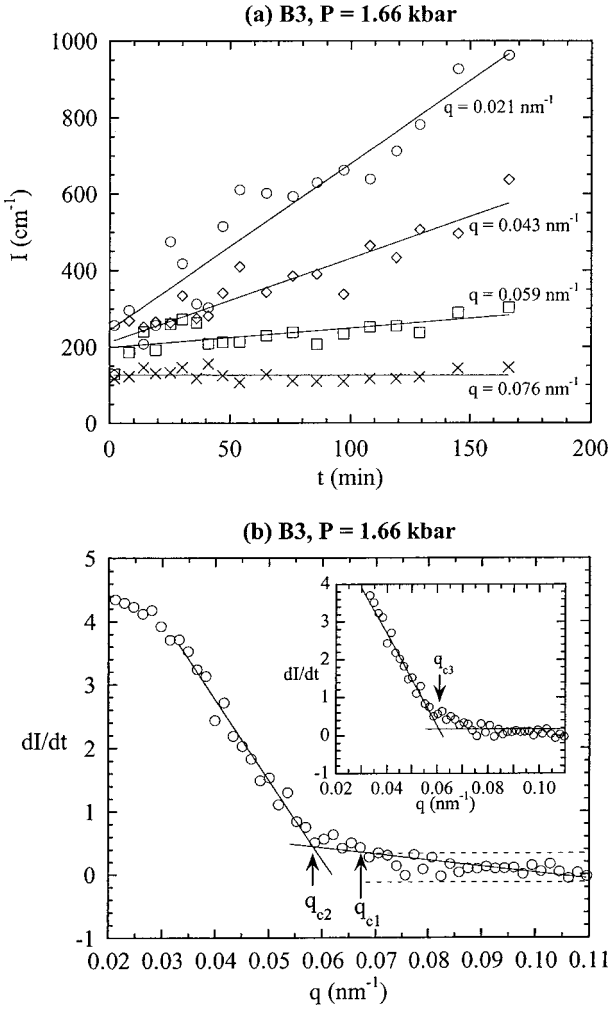

FIG. 6. (a) The time dependence of the scattering intensity, I, at selected q for the 1.66 kbar quench on B3. The lines are the best least-squares linear fits through the data. The slope of the line yields dI/dt. (b) The q-dependence of dI/dt for the 1.66 kbar quench on B3. The location of q_{c1} was determined using the standard deviation procedure. The dashed lines are twice the standard deviation of the mean intensity at $q>q_{c1}$. The solid lines are the best two least-squares lines going through the data. The intersection of these lines yields the location of q_{c2}. Inset: The q-dependence of dI/dt for the 1.66 kbar quench on B3. The solid lines through the data are the best two least-squares lines where the slope of the line through the high-q data equals zero. The intersection of these lines yields q_{c3}.

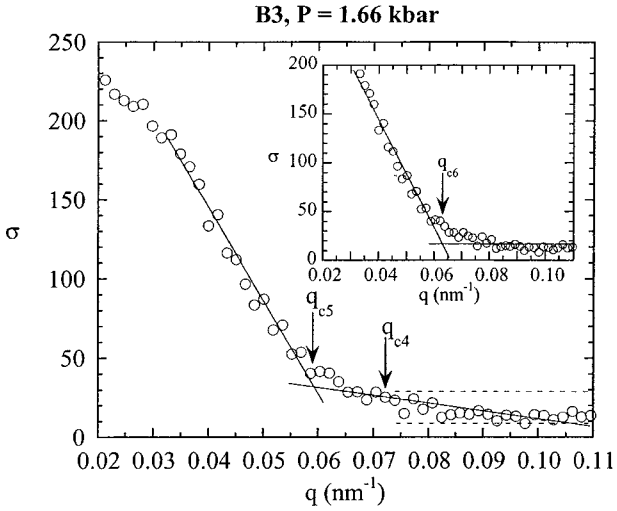

FIG. 7. The q-dependence of σ, the standard deviation of I during the early stage at a given q for the 1.66 kbar quench on B3. The location of q_{c4} was determined using the standard deviation procedure. The dashed lines are twice the standard deviation of the mean intensity at $q>q_{c4}$. The solid lines are the best two least-squares lines going through the data. The intersection of these lines yields the location of q_{c5}. Inset: The q-dependence of σ for the 1.66 kbar quench on B3. The solid lines through the data are the best two least-squares lines where the slope of the line through the high-q data equals zero. The intersection of these lines yields q_{c6}.

q_{merge} to describe this q value. The time dependence of q_{merge} thus obtained from sample B1 quenched to 0.34 kbar is shown in Fig. 8(b).[55] It is evident that q_{merge} is more-or-less time independent for $t<\tau_E$, and q_{merge} increases with time for $t>\tau_E$. We thus see that the changes in SANS profiles during the early stages ($t<\tau_E$) are similar to those depicted in Fig. 1(a). This enables the determination of a time-independent critical scattering vector q_c. As phase separation proceeds, the scattering from the phase separated structure overwhelms the scattering from concentration fluctuations at $t=0$ and we observe the scattering signature described in Fig. 1(c). In this stage, the merging of scattering curves is of little significance since it only reflects the q value at which the scattering from the two-phase structure equals the scattering from the background. The scattering signature described in Fig. 1(b), indicating a crossing of scattering curves at q_c was not evident in any of our experiments.[56]

IV. DEPENDENCE OF q_c ON QUENCH DEPTH

Following the arguments given in the Introduction and in Refs. 16 and 17, we define the critical length scale $R_c=1/q_c$. In Fig. 9 we show the dependence of the critical length scale on quench depth by plotting $(R_g/R_c)^2$ versus χ/χ_s for all three blends, where R_g, the radius of gyration of the homopolymers used in this work, equals 16 ± 1 nm. The error bars shown in Fig. 9 are calculated from the standard deviation of the six q_c values determined by the methods given in the preceding section.

Cahn and Hilliard developed an extension of the classical nucleation theory for metastable systems very close to the spinodal curve.[5] They found that in order for spontaneous growth of the new phase to occur, the initial nuclei were required to exceed a critical size. However unlike in the classical theory, the initial nuclei in Cahn and Hilliard's theory did not have the same composition as the composition of the new stable phase nor was it uniform. Their theory provided equations for the dependence of both the critical size and composition of the initial nuclei on quench depth close to the spinodal curve. The equation for the dependence of R_c on quench depth by Cahn and Hilliard is[5,57]

$$\left(\frac{R_g}{R_c}\right)^2=\left(\frac{2\chi N}{0.73}\right)^2\phi(1-\phi)\left(\frac{1}{2}-\frac{1}{2}\sqrt{1-\frac{2}{\chi N}}-\phi\right)\times\left(\sqrt{1-\frac{2}{\chi N}}\right)\quad(\chi/\chi_s<1,\ \text{i.e., nucleation}).\tag{6}$$

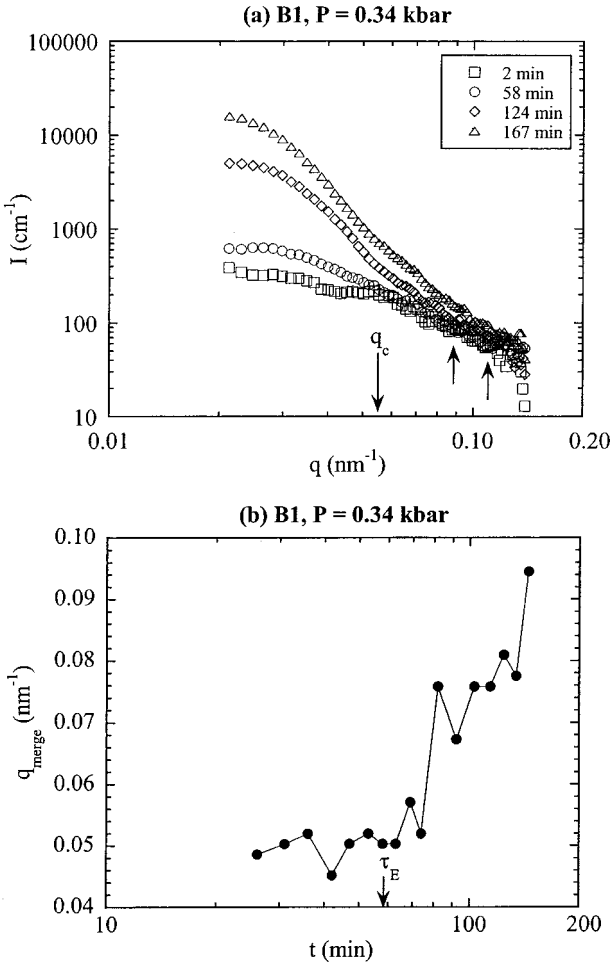

FIG. 8. (a) The SANS profiles obtained during the phase separation experiment at 0.34 kbar on the B1 sample at selected times. The arrows indicate the location of the merge point at each time. (b) The time dependence of q_{merge} for the 0.34 kbar quench on B1. The arrow indicates the end of the early stage of phase separation.

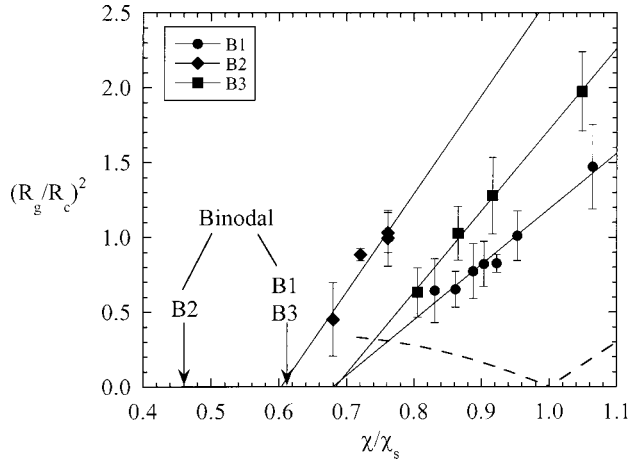

FIG. 9. A plot of $(R_g/R_c)^2$ vs quench depth, χ/χ_s, for all three blends where R_g is the radius of gyration of the polymers, R_c is the critical length scale for the developing two-phase structure, χ is the Flory–Huggins interaction parameter at the quench T and P, and χ_s is the Flory–Huggins parameter at the spinodal. The error bars in $(R_g/R_c)^2$ are due to the error in the location of q_c. The solid lines are the best least-squares linear fits through the data. The dashed curves are the theoretical predictions for blend B2 [Eqs. (6) and (7)]. The arrows indicate the value of χ/χ_s at the binodal for the three blends.

The composition of the initial structures formed during phase separation is outside the scope of this work, and thus this aspect of the theory is not addressed.

For systems located in the unstable region of the phase diagram where phase separation occurs by spinodal decomposition, Cahn predicted that[22]

$$\left(\frac{R_g}{R_c}\right)^2 = 3\left(\frac{\chi}{\chi_s} - 1\right) \qquad (\chi/\chi_s > 1, \text{ i.e., spinodal decomposition}). \quad (7)$$

The dashed curves in Fig. 9 are the theoretical prediction for the dependence of $(R_g/R_c)^2$ on quench depth using Eqs. (6) and (7).[58] It is evident that the Cahn–Hilliard theory predicts that R_c increases with increasing quench depth in the nucleation regime $(\chi/\chi_s > 1)$. This leads to a discontinuity at the spinodal. In contrast, we find that R_c decreases with increasing quench depth, and there is no discontinuity at the spinodal (Fig. 9). The solid lines through our experimental measurements in Fig. 9 are least-squares linear fits. Extrapolations based on these fits give experimental estimates of χ/χ_s where R_c may diverge. These estimates are 0.68 for B1, 0.60 for B2, and 0.68 for B3 and are indicated by the arrows in Fig. 9.

The data in Fig. 9 indicate that either the theories of phase separation kinetics of polymer blends in metastable and unstable systems are incorrect or that the equilibrium properties of polymer blends are not as well understood as commonly believed. The phase diagrams for the blends used in this work were calculated using the Flory–Huggins theory using parameters given in Tables III and IV.[59–62] The resulting binodal and spinodal curves are shown in χN versus ϕ_{PMB} format in Figs. 10(a) and 10(b). The experimental signatures and significance of these curves is discussed in Refs. 44 and 45.

It is recognized that mean-field theories such as the Flory–Huggins theory are limited to systems where the effects of concentration fluctuations are negligible. Mean-field theories thus break down near the spinodal (curves labeled S in Fig. 10), the locus of points where the characteristic length and amplitude of the concentration fluctuations are predicted to diverge. The Ginzburg number (Gi) is a measure of the relative importance of concentration fluctuations on thermodynamics.[63,64] For high molecular weight polymers, de Gennes showed that $\mathrm{Gi} \sim 1/N$, which suggests that Gi is small for large N.[65] This led to the conclusion that mean-field behavior was expected in polymer blends except for very thin regions near the spinodal (the ''width'' of these regions is of order $1/N$). The validity of this conclusion rests on the answers to the following questions: (1) What is the value of N at which the de Gennes scaling is obtained? (2) What is the prefactor of the $\mathrm{Gi} \sim 1/N$ scaling?

Wang and Wood[12,39] conducted a systematic study of the influence of concentration fluctuations on the phase diagram of polymer blends.[39] They calculated the characteristics of

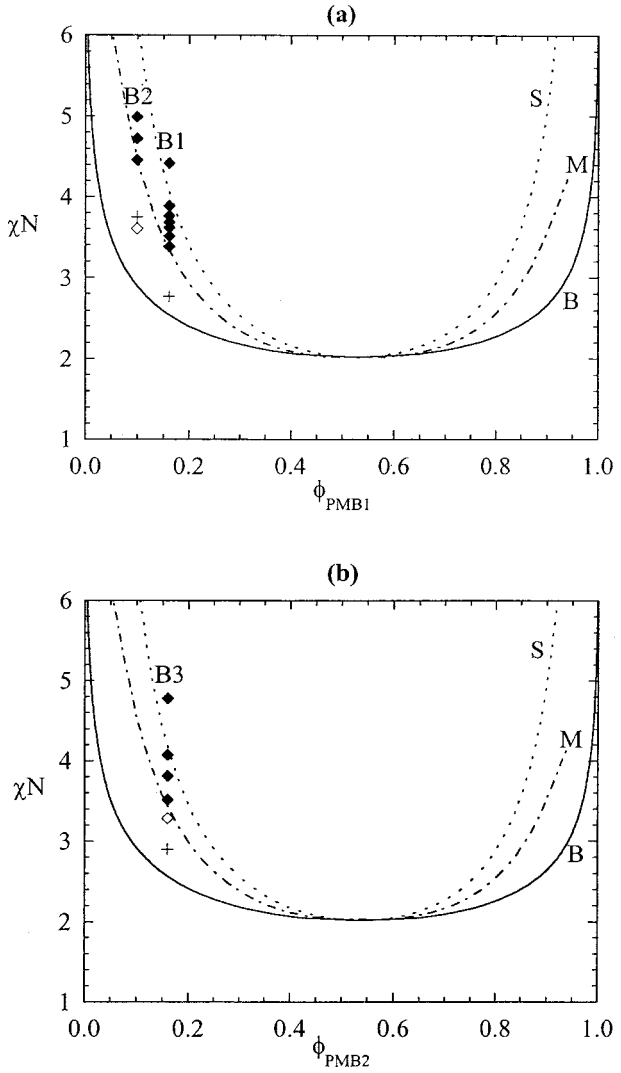

FIG. 10. The calculated $\chi N-\phi$ phase diagrams for the (a) B1 and B2, and (b) B3 blends where $N=3809$ for (a) and $N=3704$ for (b). The solid curve (B) is the mean-field binodal curve, the dashed curve (S) is the mean-field spinodal curve, and the dot–dashed curve (M) is the metastability limit proposed by Wang and Wood (Refs. 12, 39). The values of χN for the quenches where phase separation was observed and where it was not observed are indicated by the solid and open diamonds, respectively. The pluses indicate the χN value where R_c diverges, as determined from the lines in Fig. 9.

blends with $\phi_1=0.16$ and $N\approx 3000$ (corresponding to blends B1 and B3) and found that (1) the onset of the $\mathrm{Gi}\sim 1/N$ scaling occurs only at $N>10^5$, and (2) the prefactor in the $\mathrm{Gi}\sim 1/N$ scaling law is of order 10^4. They thus provided quantitative answers for the two questions raised above. These answers lead to the surprising conclusion that the role of fluctuations is important over wide regions of the phase diagram of high molecular weight polymer blends ($N\approx 3000$). In the Wang–Wood theory, the length scale (and amplitude) of the concentration fluctuations reach a finite maximum at finite quench depths below the binodal. The locus of points corresponds to this maximum, is called the pseudospinodal in Ref. 39. The pseudospinodal is thus interpreted as the limit of metastability for a binary polymer blend. The analytical expression for χ_{ml} (χ at the metastability limit) is[39]

$$\chi_{\mathrm{ml}}=\chi_s\left\{1-2.5\left(\frac{l_1 l_2}{\bar{l}}\right)\frac{(V_1V_2)^{1/3}}{\bar{V}}\times\left[\frac{((1-\phi_1)^2V_2-\phi_1^2V_1)^2}{\phi_1(1-\phi_1)V_1V_2}\right]^{2/3}\right\}, \tag{8}$$

where $V_i=N_i v_i$, $l_i=V_i/R_i^2$, $\bar{V}=\phi_1V_1+(1-\phi_1)V_2$, $\bar{l}=\phi_1 l_1+(1-\phi_1)l_2$, R_i is the end-to-end distance of polymer i and is given by $R_i^2=N_i l_{i,\mathrm{ref}}^2$. The curve labeled M in Fig. 10 is the metastability limit ($\chi_{\mathrm{ml}}N$ vs ϕ_{PMB}), calculated using Eq. (8). All of the parameters required to compute the metastability limit have been measured independently and are given in Table IV.

The relationship between χ_{ml} and our experiments is shown in Fig. 10. The solid diamonds indicate the values of χN for each of the quenches where we observed phase separation. All of these quenches are deeper than the calculated metastability limit.[66] The values of χN for the two quenches where we did not observe phase separation, during the time scale of our experiments (18 h), are shown by the open diamonds. These two quenches are shallower than the metastability limit. *Thus, the theoretical and experimental metastability limits are in quantitative agreement.* This agreement, which was also noted by Wang in Ref. 39, is obtained without any adjustable parameters. The terms pseudospinodal and metstability limit are thus interchangeable. It is worth noting that the experimental conclusions are based on *kinetic* data obtained from quenches *deeper* than the metastability limit, while the theory only addresses the *equilibrium* properties of systems at quench depths that are *shallower* than the metastability limit. The values of χN, where R_c diverges,[67] indicated by the plus signs in Fig. 10, lie between the binodal and the metastability limit.

The Wang–Wood theory provides an explanation for the departure between theory and experiment seen in Fig. 9. Since our phase separation experiments were conducted in the regime where the Ginzburg number is large, the kinetics of phase separation must be effected by concentration fluctuations. Such fluctuation-mediated phase separation is outside the scope of the Cahn–Hilliard theory.[5,22] A detailed understanding of the dependence of the critical length scales on quench depth (Fig. 9) requires theories that capture the role of fluctuations during phase separation in systems beyond the metastability limit.

V. CONCLUDING REMARKS

The main purpose of this study was to use blends of high molecular weight polymers as model systems for studying the initial stages of nucleation in metastable systems. We found that the scattering signature for the critical length scale, R_c, of the initial structures formed during phase separation was a time independent critical scattering vector, q_c, and $R_c=1/q_c$. We have established methods for determining R_c. We found that R_c decreases with *decreasing* quench depth and diverged between the binodal and spinodal curves. This result is not in agreement with well-established classical theories dealing with polymer blend thermodynamics and phase separation kinetics. The reason for the lack of agree-

ment is addressed in the recent theories of Wang and Wood[12,39] who showed that our experiments were carried out in a regime where the phase behavior is strongly effected by concentration fluctuations.

ACKNOWLEDGMENTS

We thank Boualem Hammouda for his assistance in all aspects of this work, and Zhen-Gang Wang for educational discussions about thermodynamics and nucleation. This work is supported by the National Science Foundation (Grant No. CTS-0196066). We acknowledge the support of the National Institute of Standards and Technology, U.S. Department of Commerce, in providing the facilities used in this work. The SANS instrument is supported by Grant No. DMR-9986442 from the National Science Foundation to the NIST (Ref. 68).

[1] J. W. Gibbs, *The Scientific Papers of J. Willard Gibbs* (Dover, New York, 1961).
[2] R. Becker and W. Doring, Ann. Phys. (Leipzig) **24**, 719 (1935).
[3] J. D. Gunton, M. San Miguel, and P. S. Sahani, in *Phase Transitions* (Academic, New York, 1983), Vol. 8.
[4] P. G. Debenedetti, *Metastable Liquids: Concepts and Principles* (Princeton University Press, Princeton, 1996).
[5] J. W. Cahn and J. E. Hilliard, J. Chem. Phys. **31**, 688 (1959).
[6] K. Binder and D. Stauffer, Adv. Phys. **25**, 343 (1976).
[7] A. Sur, J. L. Lebowitz, J. Marro, and M. H. Kalos, Phys. Rev. B **15**, 3014 (1977).
[8] J. S. Langer and A. J. Schwartz, Phys. Rev. A **21**, 948 (1980).
[9] K. Binder, J. Chem. Phys. **79**, 6387 (1983).
[10] D. W. Heermann and W. Klein, Phys. Rev. B **27**, 1732 (1983).
[11] K. Binder, Phys. Rev. A **29**, 341 (1984).
[12] S. M. Wood and Z. G. Wang, J. Chem. Phys. **116**, 2289 (2002).
[13] S. Krishnamurthy and W. I. Goldburg, Phys. Rev. A **22**, 2147 (1980).
[14] A. Cumming, P. Wiltzius, F. S. Bates, and J. H. Rosedale, Phys. Rev. A **45**, 885 (1992).
[15] K. Schatzel and B. J. Ackerson, Phys. Rev. E **48**, 3766 (1993).
[16] A. A. Lefebvre, J. H. Lee, N. P. Balsara, and B. Hammouda, J. Chem. Phys. **116**, 4777 (2002).
[17] A. A. Lefebvre, J. H. Lee, H. S. Jeon, N. P. Balsara, and B. Hammouda, J. Chem. Phys. **111**, 6082 (1999).
[18] N. P. Balsara, C. C. Lin, and B. Hammouda, Phys. Rev. Lett. **77**, 3847 (1996).
[19] S.-T. Yau and P. G. Vekilov, Nature (London) **406**, 494 (2000).
[20] U. Gasser, E. R. Weeks, A. Schoefield, P. N. Pusey, and D. A. Weitz, Science **292**, 258 (2001).
[21] We showed in Ref. 17 that the growing structures were self-similar, regardless of time and quench depth. Thus, the prefactor must be the same for all of the quenches.
[22] J. W. Cahn, Trans. Metall. Soc. AIME **242**, 166 (1968).
[23] J. W. Cahn, J. Chem. Phys. **42**, 93 (1965).
[24] K. B. Rundman and J. E. Hilliard, Acta Metall. **15**, 1025 (1967).
[25] N-C. Wong and C. M. Knobler, J. Chem. Phys. **69**, 725 (1978).
[26] Y. C. Chou and W. I. Goldburg, Phys. Rev. A **23**, 858 (1981).
[27] M. Okada and C. C. Han, J. Chem. Phys. **85**, 5317 (1986).
[28] F. S. Bates and P. Wilzius, J. Chem. Phys. **91**, 3258 (1989).
[29] D. Schwahn, S. Janssen, and T. Springer, J. Chem. Phys. **97**, 8775 (1992).
[30] H. Jinnai, H. Hasegawa, T. Hashimoto, and C. C. Han, J. Chem. Phys. **99**, 4845 (1993).
[31] J. S. Higgins and H. C. Benoît, *Polymers and Neutron Scattering* (Oxford University Press, Oxford, 1994).
[32] C. C. Lin, H. S. Jeon, N. P. Balsara, and B. Hammouda, J. Chem. Phys. **103**, 1957 (1995).
[33] B. Hammouda, N. P. Balsara, and A. A. Lefebvre, Macromolecules **30**, 5572 (1997).
[34] Y. Xiong and E. Kiran, Rev. Sci. Instrum. **69**, 1463 (1998).
[35] P. G. de Gennes, *Scaling Concepts in Polymer Physics* (Cornell University Press, Ithaca, 1979).
[36] K. Binder, J. Chem. Phys. **79**, 6387 (1983).
[37] P. Pincus, J. Chem. Phys. **75**, 1996 (1981).
[38] A. A. Lefebvre, J. H. Lee, N. P. Balsara, and C. Vaidyanathan, J. Chem. Phys. **117**, 9074 (2002).
[39] Z. G. Wang, J. Chem. Phys. **117**, 481 (2002).
[40] H. Rachapudy, G. G. Smith, V. R. Raju, and W. W. Graessley, J. Polym. Sci., Polym. Phys. Ed. **17**, 1211 (1979).
[41] M. Morton and L. J. Fetters, Rubber Chem. Technol. **48**, 359 (1975).
[42] R. Krishnamoorti, Ph.D. thesis, Princeton University, Princeton, NJ, 1994.
[43] N. P. Balsara, S. V. Jonnalagadda, C. C. Lin, C. C. Han, and R. Krishnamoorti, J. Chem. Phys. **99**, 10011 (1993).
[44] A. A. Lefebvre, J. H. Lee, N. P. Balsara, and B. Hammouda, Macromolecules **33**, 7977 (2000).
[45] A. A. Lefebvre, J. H. Lee, N. P. Balsara, and C. Vaidyanathan, Macromolecules **35**, 7758 (2002).
[46] C. C. Lin, S. V. Jonnalagadda, N. P. Balsara, C. C. Han, and R. Krishnamoorti, Macromolecules **29**, 661 (1996).
[47] A. A. Lefebvre, Ph.D. thesis, University of California, Berkeley, CA, 2002.
[48] A. A. Lefebvre, J. H. Lee, N. P. Balsara, and B. Hammouda, J. Polym. Sci., Polym. Phys. Ed. **38**, 1926 (2000).
[49] A. A. Lefebvre, J. H. Lee, N. P. Balsara, B. Hammouda, R. Krishnamoorti, and S. Kumar, Macromolecules **32**, 5460 (1999).
[50] N. P. Balsara, A. A. Lefebvre, J. H. Lee, C. C. Lin, and B. Hammouda, AIChE J. **44**, 2515 (1998).
[51] R. Krishnamoorti, W. W. Graessley, N. P. Balsara, and D. J. Lohse, Macromolecules **27**, 3073 (1994).
[52] Two independent runs were conducted on B2 at 35 °C. The fluctuation relaxation stage was clearly identified in only one of the runs.
[53] For the 2.00 and 3.10 kbar quenches on B3, we began the standard deviation procedure at $q=0.14$ and $0.12\ \mathrm{nm}^{-1}$, respectively. We were able to begin the standard deviation procedure at higher q, because the detector was offset for these two experiments. This allowed measurements of the scattering intensity at higher q.
[54] The data at $q<0.033\ \mathrm{nm}^{-1}$ were not included in the fitting procedure, because the q dependence of dI/dt in this regime is different than in the $0.033<q<0.060\ \mathrm{nm}^{-1}$ range.
[55] Quantitative determination of the location of q_{merge} at both very early and late times was not possible. At early times, the small increases in the scattering intensity were of the same order as the noise in the data. At late times, the merge point moved to q-values near the high q limit of our SANS instrument.
[56] This includes earlier work on multicomponent polymer blends described in Refs. 16–18.
[57] Equations (6) and (7) apply to a blend of polymers with the same N_i and R_g. In our blends R_g is the same $(16\pm1\ \mathrm{nm})$, but N_i are different. We take N to be the average value of N_i (3809 for B1 and B2, and 3704 for B3) in our comparisons of theory and experiment.
[58] The theoretical curves for the three blends are nearly indistinguishable in the range of interest (ordinate difference is <0.03). For simplicity, a single curve (the average between the three theoretical curves) is shown.
[59] A. J. Staverman and J. H. Van Saten, Recl. Trav. Chim. Pays-Bas. **60**, 76 (1941).
[60] P. J. Flory, J. Chem. Phys. **10**, 51 (1942).
[61] M. L. Huggins, J. Phys. Chem. **46**, 151 (1942).
[62] The $\chi-\phi_{\mathrm{PMB}}$ phase diagrams were calculated using $N_{\mathrm{PMB1}}=3357$, $N_{\mathrm{PMB2}}=3147$, $N_{\mathrm{PEB1}}=N_{\mathrm{PEB2}}=4260$ and $v_{\mathrm{PMB1}}=v_{\mathrm{PMB2}}=v_{\mathrm{PEB1}}=v_{\mathrm{PEB2}}=100\ \mathrm{Å}^3$. The binodal, spinodal, and pseudospinodal curves in Figs. 10(a) and 10(b) were obtained by multiplying χ by the average value of N_i [3809 for Fig. 10(a) and 3704 for Fig. 10(b)]. Thus the small changes in the monomer volumes with changing T and P are not accounted for in this figure.
[63] V. L. Ginzburg, Sov. Phys. Solid State **2**, 1824 (1960).
[64] A. P. Levanyuk, Sov. Phys. JETP **36**, 571 (1959).
[65] P. G. de Gennes, J. Phys. (France) Lett. **38**, L-441 (1977).
[66] The 45 °C quench on the B2 sample lay just outside, but within experimental error of the pseudospinodal.
[67] The values of χN for the divergence point were obtained by multiplying the value of χ/χ_s where $(R_g/R_c)^2=0$ in Fig. 9 by the value of χ_s at the spinodal in Fig. 10 (B1: $\chi_s=0.00107$, B2: $\chi_s=0.00164$, and B3: $\chi_s=0.00782$) and the average value of N (3809 for B1 and B2 and 3704 for B3).
[68] Identification of equipment and materials does not imply recommendation by the National Institute of Standards and Technology.